nature portfolio

https://doi.org/10.1038/s41567-021-01345-6

Supplementary information

Oscillating features in the electromagnetic structure of the neutron

In the format provided by the authors and unedited

Supplementary Materials

Note: Figures, Tables, References, and Equations from the Supplementary Materials are indicated accordingly.

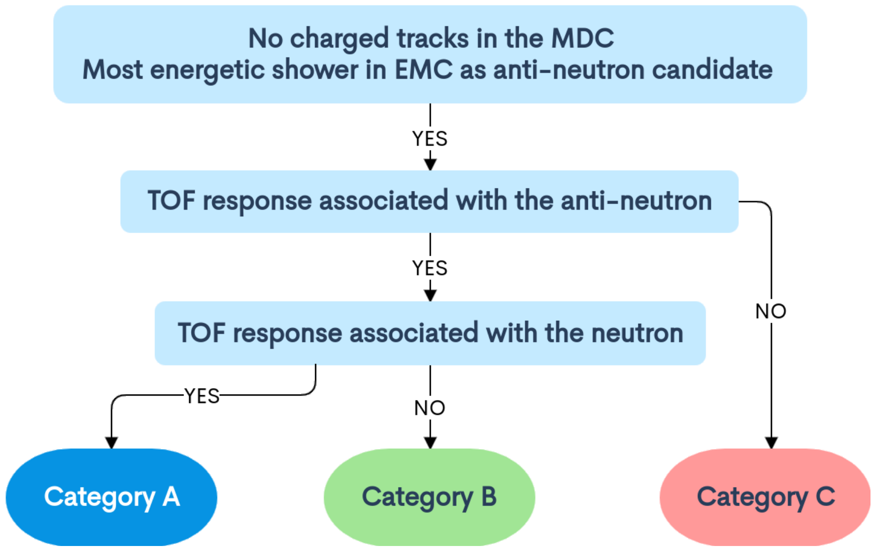

Supplementary Figure 1: Classification logic for the signal selection. The signal process is reconstructed from events without charged tracks. The most energetic EMC response in the event is identified as from the antineutron. If a TOF response can be matched to the antineutron response in the EMC, the event is classified as category A or B, else as C. If a TOF response is reconstructed at the opposite side of the detector with respect to the antineutron in the EMC, the event is categorized as A, else as B.

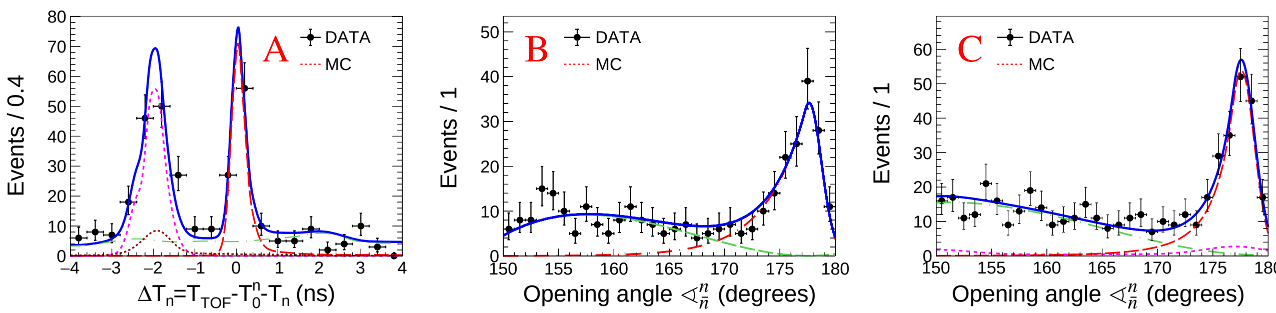

Supplementary Figure 2: Examples for the extraction of reconstructed signal events N_s from the pre-selected data sample at the c.m. energy $\sqrt{s} = 2.396$ GeV. The reconstructed events of three sub-sets of the data are presented depending on the corresponding detector impact as a function of (A) ΔT_n and (B, C) $\sphericalangle_{\bar{n}}^{n}$, where ΔT_n is the difference between the measured and expected time-of-flight of the neutron in the TOF, $\sphericalangle_{\bar{n}}^{n}$ is opening angle between the anti-neutron and neutron showers in the EMC. The logic for the classification into the three sub-sets of data is shown in the Supplementary Figure 1. Black dots with errors indicate BESIII data. The red, green, pink, brown, and blue lines show the signal-, beam-related and cosmic ray-, multi-hadronic-, and di-gamma background components, and the total fit based on Equation 2, respectively. For all data points the shown uncertainty is statistical and corresponds to a 68.3% confidence level of a normal distribution.

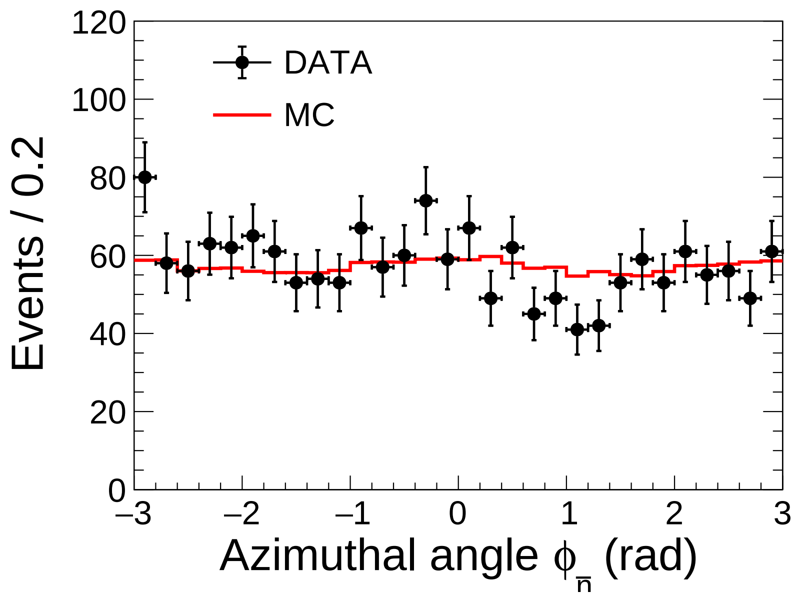

Supplementary Figure 3: The azimuthal angle distribution of the anti-neutron in the EMC (black: data, red: MC) as a sum from the three categories A, B, and C, and all energies with additional cut criteria to reject the remaining background (category A: difference between the measured and expected flight time of the neutron $-0.5 < |\Delta T_n| < 1$ (ns), category B and C: the opening angle between the neutron and anti-neutron in the EMC $\sphericalangle_{\bar{n}}^{n} > 175^\circ$ - for comparison see Supplementary Figure 2). The data is shown at observation level without any corrections applied. The number of events in the MC simulation is scaled to the number of events in data. For all data points the shown uncertainty is statistical and corresponds to a 68.3% confidence level of a normal distribution.

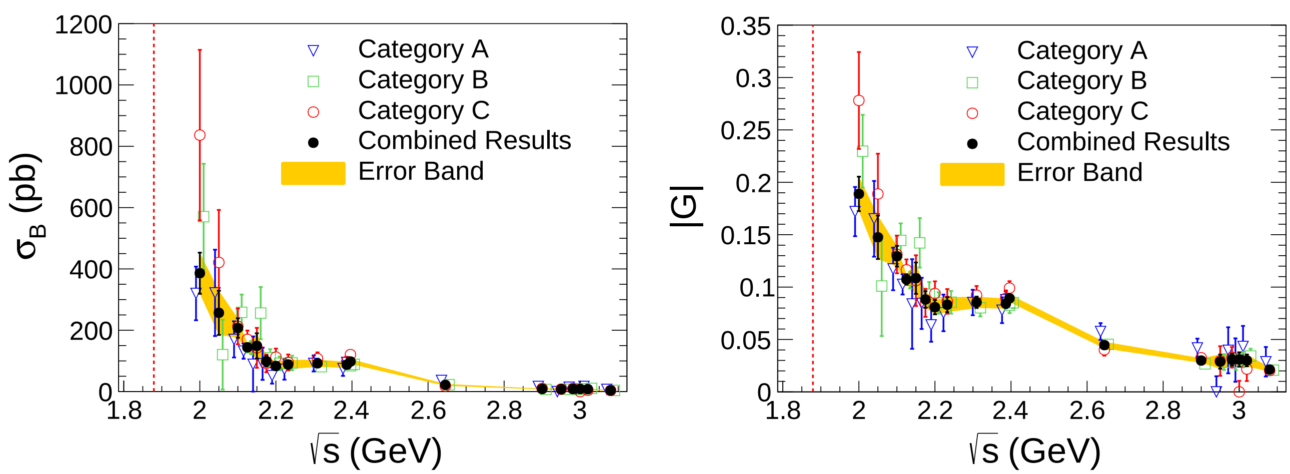

Supplementary Figure 4: Comparison of the results for (left) the Born cross section σ_B and (right) the effective form factor $|G|$ for the process $e^+e^- \to n\bar{n}$ from the three signal classification categories. Results shown in blue, green and red are extracted with the signal classification category A, B, and C, respectively, each with statistical uncertainty only. The black circles are the combined results using the formula from Equation 4. The yellow bands represent the statistical uncertainty of the combined results as listed in Table 1 of the main text. The individual results are listed in the Supplementary Tables 1 - 3. The results for the category A and B have been shifted by $\sqrt{s} =$ -0.01 and 0.01 for a better visual representation. For all data points the shown uncertainty is statistical and corresponds to a 68.3% confidence level of a normal distribution.

Supplementary Table 1: Category A: Summary of the results for σ_B^A, $|G^A|$, and the related quantities at each $\sqrt{s}$. The first uncertainty is statistical and the second one systematic. The columns show the c.m. energy $\sqrt{s}$, the number of signal events N_A^s, the luminosity $\mathscr{L}_{\rm int}$, the MC selection efficiency ε_{MC}^A, and the efficiency correction factors $\mathscr{C}_{n\bar{n}}^A$ and $\mathscr{C}_{trg}^A$.

$\sqrt{s}$ (GeV)	N_A^s	$\mathscr{L}_{\rm int}$ (pb^{-1})	$(1+\delta)$	$\varepsilon_{MC}^A(\%)$	$\mathscr{C}_{n\bar{n}}^A(\%)$	$\mathscr{C}_{trg}^A(\%)$	σ_B^A (pb)	$\|G^A\|$ $(\times 10^{-2})$
2.0000	38.3 ± 7.3	10.1	0.98	1.35	108.3	82.9	$319 \pm 60 \pm 44$	$17.3 \pm 1.6 \pm 1.2$
2.0500	12.8 ± 4.1	3.34	1.08	1.27	104.1	83.3	$320 \pm 100 \pm 40$	$16.5 \pm 2.6 \pm 1.0$
2.1000	24.3 ± 5.7	12.2	1.18	1.23	96.5	83.8	$169 \pm 40 \pm 28$	$11.7 \pm 1.4 \pm 1.0$
2.1250	172 ± 15	108	1.24	1.19	96.3	84.6	$133 \pm 11 \pm 17$	$10.3 \pm 0.4 \pm 0.7$
2.1500	3.0 ± 2.2	2.84	1.29	1.15	93.3	85.7	$89 \pm 65 \pm 14$	$8.4 \pm 3.1 \pm 0.7$
2.1750	10.9 ± 4.1	10.6	1.31	1.09	94.4	83.8	$91 \pm 34 \pm 14$	$8.5 \pm 1.6 \pm 0.7$
2.2000	8.0 ± 3.5	13.7	1.31	1.06	94.6	85.3	$52 \pm 22 \pm 7$	$6.4 \pm 1.4 \pm 0.4$
2.2324	10.0 ± 3.9	11.9	1.28	1.08	98.8	85.1	$72 \pm 28 \pm 10$	$7.5 \pm 1.5 \pm 0.5$
2.3094	22.6 ± 5.8	21.1	1.14	1.21	96.6	87.6	$91 \pm 23 \pm 11$	$8.5 \pm 1.1 \pm 0.5$
2.3864	22.5 ± 5.8	22.5	1.11	1.40	95.9	89.3	$75 \pm 19 \pm 9$	$7.8 \pm 1.0 \pm 0.5$
2.3960	80.3 ± 9.9	66.9	1.11	1.35	94.5	89.2	$95 \pm 11 \pm 11$	$8.8 \pm 0.5 \pm 0.5$
2.6454	19.4 ± 4.7	67.7	1.55	0.64	83.8	94.7	$37 \pm 9 \pm 5$	$5.8 \pm 0.7 \pm 0.4$
2.9000	16.3 ± 4.4	105	2.16	0.56	79.9	95.9	$17 \pm 5 \pm 2$	$4.2 \pm 0.6 \pm 0.2$
2.9500	0.0 ± 1.3	15.9	2.29	0.57	77.9	96.7	$0.0 \pm 8.3 \pm 0.0$	–
2.9810	2.3 ± 1.9	16.1	2.36	0.56	78.8	95.8	$15 \pm 11 \pm 5$	$4.1 \pm 1.5 \pm 0.7$
3.0000	1.4 ± 1.3	15.9	2.41	0.57	80.2	96.0	$8.3 \pm 7.7 \pm 8.4$	$3.0 \pm 1.4 \pm 1.5$
3.0200	2.9 ± 2.1	17.3	2.46	0.55	80.0	95.7	$16 \pm 11 \pm 3$	$4.2 \pm 1.5 \pm 0.4$
3.0800	12.1 ± 4.3	126	2.61	0.56	95.8	96.5	$7.1 \pm 2.5 \pm 1.3$	$2.9 \pm 0.5 \pm 0.3$

Supplementary Table 2: Category B: Summary of the results for σ_B^B, $|G^B|$, and the related quantities at each $\sqrt{s}$. The first uncertainty is statistical and the second one systematic. The columns show the c.m. energy $\sqrt{s}$, the number of signal events N_B^s, the luminosity $\mathscr{L}_{\rm int}$, the MC selection efficiency ε_{MC}^B, and the efficiency correction factors $\mathscr{C}_{n\bar{n}}^B$ and $\mathscr{C}_{trg}^B$.

$\sqrt{s}$ (GeV)	N_B^s	$\mathscr{L}_{\rm int}$ (pb^{-1})	$(1+\delta)$	$\varepsilon_{MC}^B(\%)$	$\mathscr{C}_{n\bar{n}}^B(\%)$	$\mathscr{C}_{trg}^B(\%)$	σ_B^B (pb)	$\|G^B\|$ $(\times 10^{-2})$
2.0000	16.2 ± 4.5	10.1	0.98	0.43	76.8	86.7	$570 \pm 160 \pm 70$	$23.1 \pm 3.2 \pm 1.4$
2.0500	2.3 ± 2.1	3.34	1.08	0.86	69.6	87.2	$120 \pm 110 \pm 20$	$10.1 \pm 4.6 \pm 0.8$
2.1000	36.1 ± 6.6	12.2	1.18	1.43	76.6	88.7	$258 \pm 47 \pm 35$	$14.5 \pm 1.3 \pm 1.0$
2.1250	226 ± 17	108	1.24	1.69	77.8	89.4	$144 \pm 11 \pm 19$	$10.7 \pm 0.4 \pm 0.7$
2.1500	12.5 ± 3.8	2.84	1.28	1.91	78.0	90.3	$256 \pm 78 \pm 34$	$14.2 \pm 2.2 \pm 0.9$
2.1750	22.7 ± 5.2	10.6	1.31	2.04	81.7	88.6	$110 \pm 25 \pm 12$	$9.3 \pm 1.1 \pm 0.5$
2.2000	29 ± 5.8	13.7	1.31	2.38	81.6	90.4	$92 \pm 19 \pm 12$	$8.5 \pm 0.9 \pm 0.6$
2.2320	27.3 ± 5.9	11.9	1.28	2.56	83.1	90.5	$93 \pm 20 \pm 12$	$8.5 \pm 0.9 \pm 0.6$
2.3090	40.8 ± 6.8	21.1	1.15	2.56	85.9	94.0	$82 \pm 14 \pm 10$	$8.1 \pm 0.7 \pm 0.5$
2.3860	56.9 ± 8.0	22.5	1.11	3.20	88.7	94.8	$85 \pm 12 \pm 10$	$8.3 \pm 0.6 \pm 0.5$
2.3960	172 ± 14	66.9	1.11	3.12	88.7	94.3	$89 \pm 7 \pm 8$	$8.5 \pm 0.3 \pm 0.4$
2.6440	57.9 ± 8.2	67.7	1.55	3.02	84.0	96.3	$22 \pm 3 \pm 3$	$4.5 \pm 0.3 \pm 0.3$
2.9000	29.3 ± 5.8	105	2.17	2.40	80.7	97.2	$6.9 \pm 1.4 \pm 0.9$	$2.7 \pm 0.3 \pm 0.2$
2.9500	5.1 ± 2.6	15.9	2.29	2.34	80.7	97.7	$7.6 \pm 3.9 \pm 1.1$	$2.9 \pm 0.7 \pm 0.2$
2.9810	4.9 ± 2.5	16.1	2.36	2.22	80.7	97.3	$7.4 \pm 3.8 \pm 1.1$	$2.9 \pm 0.7 \pm 0.2$
3.0000	5.9 ± 2.6	15.9	2.41	2.24	80.7	97.5	$8.7 \pm 3.8 \pm 1.4$	$3.1 \pm 0.7 \pm 0.3$
3.0200	7.5 ± 2.8	17.3	2.46	2.14	80.7	97.4	$10 \pm 4 \pm 2$	$3.4 \pm 0.5 \pm 0.3$
3.0800	19.8 ± 4.9	126	2.61	2.08	80.0	97.8	$3.7 \pm 0.9 \pm 0.7$	$2.1 \pm 0.3 \pm 0.2$

Supplementary Table 3: Category C: Summary of the results for σ_B^C, $|G^C|$, and the related quantities at each $\sqrt{s}$. The first uncertainty is statistical and the second one systematic. The columns show the c.m. energy $\sqrt{s}$, the number of signal events N_C^s, the luminosity $\mathscr{L}_{\rm int}$, the MC selection efficiency ε_{MC}^C, and the efficiency correction factors $\mathscr{C}_{n\bar{n}}^C$, $\mathscr{C}_{trg}^C$, and $\mathscr{C}_{ee}^C$.

$\sqrt{s}$ (GeV)	N_C^s	$\mathscr{L}_{\rm int}$ (pb^{-1})	$(1+\delta)$	$\varepsilon_{MC}^C(\%)$	$\mathscr{C}_{\rm n\bar{n}}^C(\%)$	$\mathscr{C}_{\rm trg}^C(\%)$	$\mathscr{C}_{\rm ee}^C(\%)$	σ_B^C (pb)	$\|G^C\|$ $(\times 10^{-2})$
2.0000	25.8 ± 6.0	10.1	0.98	0.34	137.5	88.8	75.0	$840\pm200\pm200$	$28.0\pm3.3\pm3.3$
2.0500	9.8 ± 3.5	3.34	1.08	0.75	126.7	91.1	75.2	$420\pm150\pm90$	$18.9\pm3.4\pm2.0$
2.1000	31.3 ± 6.2	12.2	1.18	1.15	125.4	92.1	77.3	$212\pm42\pm41$	$13.1\pm1.3\pm1.3$
2.1266	281 ± 18	108	1.24	1.34	124.7	92.5	79.8	$170\pm11\pm27$	$11.7\pm0.4\pm0.9$
2.1500	7.4 ± 3.1	2.84	1.28	1.51	123.5	92.9	83.0	$142\pm59\pm27$	$10.6\pm2.2\pm1.0$
2.1750	19.7 ± 5.4	10.6	1.31	1.59	123.4	91.8	86.0	$92\pm25\pm14$	$8.5\pm1.2\pm0.7$
2.2000	35.2 ± 6.9	13.7	1.31	1.74	123.1	92.3	88.1	$113\pm22\pm17$	$9.4\pm0.9\pm0.7$
2.2324	27.4 ± 6.0	11.9	1.28	1.89	121.6	92.9	89.2	$94\pm20\pm15$	$8.6\pm0.9\pm0.7$
2.3094	52.3 ± 8.1	21.1	1.14	1.93	122.7	95.0	89.6	$108\pm17\pm12$	$9.3\pm0.7\pm0.5$
2.3864	57.0 ± 8.0	22.5	1.11	2.32	116.7	95.9	89.7	$98\pm14\pm9$	$8.9\pm0.6\pm0.4$
2.3960	212 ± 16	66.9	1.11	2.36	116.7	95.8	89.7	$121\pm9\pm13$	$9.9\pm0.4\pm0.5$
2.6454	44.1 ± 8.6	67.7	1.55	2.74	100.6	97.1	89.8	$17\pm3\pm4$	$4.1\pm0.3\pm0.5$
2.9000	47.5 ± 8.5	105	2.16	2.28	103.2	97.6	90.0	$10\pm2\pm2$	$3.2\pm0.3\pm0.3$
2.9500	6.1 ± 3.3	15.9	2.29	2.25	104.6	98.0	90.1	$8.1\pm4.4\pm6.4$	$3.0\pm0.8\pm1.2$
2.9810	7.5 ± 3.8	16.1	2.36	2.16	104.8	97.7	90.1	$9.9\pm5.0\pm3.0$	$3.3\pm0.8\pm0.5$
3.0000	0 ± 3.0	15.9	2.41	2.11	105.6	97.7	90.1	$0.0\pm4.0\pm0.0$	–
3.0200	3.4 ± 3.4	17.3	2.46	2.06	105.7	97.8	90.1	$4.2\pm4.2\pm1.4$	$2.2\pm1.1\pm0.4$
3.0800	21.0 ± 6.2	126	2.61	1.93	105.9	97.9	90.2	$3.5\pm1.0\pm1.0$	$2.0\pm0.3\pm0.3$

Verification of the Time-of-Flight Reconstruction Efficiency

The Supplementary Figure 5 shows the verification of the reconstruction efficiency for the time-of-flight measurement for neutral particles with the process $e^+e^- \to J/\psi \to \pi^+\pi^-\pi^0$, as described in **Methods**.

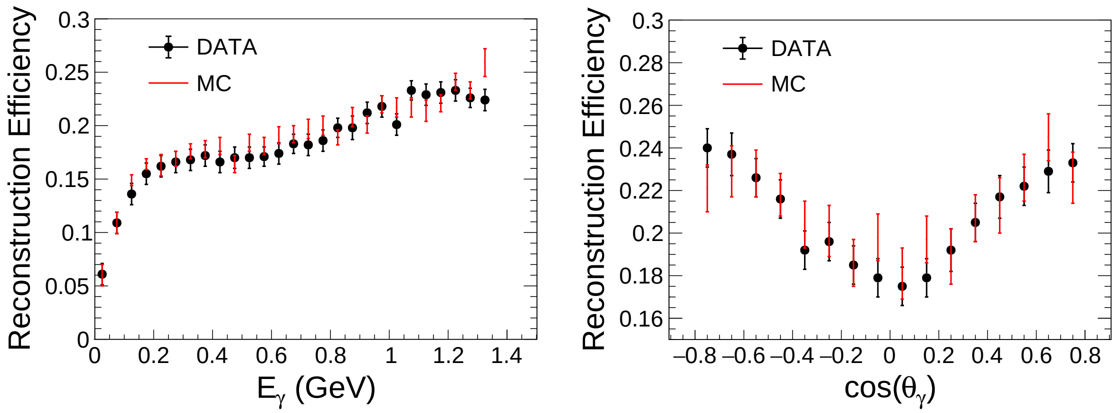

Supplementary Figure 5: Reconstruction efficiency for a photon using the neutral TOF algorithm (left) as a function of the deposition energy in the EMC with values for the cosine of the polar angle $\cos\theta$ within (−0.8, 0.8), and (right) as a function of $\cos\theta$ with values for the deposition energy within (0.80, 1.20) GeV. Results from data and MC are shown as black dots and red lines. The uncertainties are statistical and correspond to a 68.3% confidence level of a normal distribution.

The process $e^+e^- \to \gamma\gamma$ is used to verify the reconstruction for the time-of-flight measurement for neutral particles. The selection criteria are as follows: the event must contain no charged tracks and at least one shower in the EMC, the most energetic shower must be within $|\cos\theta| < 0.8$, the difference between the measured and expected flight time for the most energetic EMC shower and the second TOF hit must be within $|T^\gamma_{TOFi} - T^\gamma_{exp}| < 1$ ns ($i = 1, 2$), the deposition energy of the most energetic EMC shower E_1 must be within $0.7\sqrt{s}/2 < E_1 < 1.1\sqrt{s}/2$ (GeV). The time difference between the measured time of two showers must be within $|T^\gamma_{TOF1} - T^\gamma_{TOF2}| < 1$ ns considering the identical features of two photons. The open angle between the position vector of the leading energetic shower and the measured position vector of the second TOF must be larger than 3.0 radian. The results are shown in the Supplementary Table 4.

Supplementary Table 4: Verification of the reconstruction efficiency for the neutral TOF algorithm with the process $e^+e^- \to \gamma\gamma$. The luminosity is quoted from the References [18, 19], the reference Born cross section σ_{ref} is taken from the BABAYAGA generator as quoted in Reference [36], the reconstruction efficiency $\varepsilon^{\gamma\gamma}_{MC}$ is determined from dedicated signal MC samples generated with BABAYAGA, the observed cross section is determined as $\sigma_{obs} = N_{\gamma\gamma}/(\mathscr{L}\varepsilon^{\gamma\gamma}_{MC})$. The uncertainties are statistical.

$\sqrt{s}$ (GeV)	$\mathscr{L}$ (pb^{-1}) [18, 19]	$\varepsilon^{\gamma\gamma}_{MC}$(%)	$N_{\gamma\gamma}$	σ_{obs} (nb)	σ_{ref} (nb) Reference [36]
2.0000	10.1	2.0	17808	87.6 ± 0.7	88.0 ± 0.9
2.1250	108	2.0	167428	76.2 ± 0.2	77.4 ± 0.3
2.1750	10.6	2.0	15737	72.9 ± 0.6	74.6 ± 0.3
2.2000	13.7	2.0	19867	71.2 ± 0.5	72.5 ± 0.3
2.2324	11.9	2.0	16827	69.7 ± 0.5	70.5 ± 0.3
2.3960	66.9	2.0	82185	60.2 ± 0.2	61.1 ± 0.3
2.6444	33.7	2.1	67623	48.4 ± 0.2	50.0 ± 0.2
2.9000	105	2.1	89826	41.2 ± 0.1	41.7 ± 0.2
3.0800	126	2.1	95549	36.8 ± 0.1	37.2 ± 0.2

Using the Muon Counter as Veto Against Beam-related and Cosmic Background

The MUC is used as a veto against beam-related and cosmic background in this analysis. For most analyses at BESIII the beam-related and cosmic background doesn't play any role, since it is effectively suppressed by the MDC and TOF trigger sub-systems ($> 99\%$) as described in the Reference [15] (page 46, table 27). The situation differs for events with pure neutral final states, where only the EMC sub-trigger is activated. The rate for cosmic rays is estimated to be 1.5 kHz and the rate of lost particles in the detector, assuming an uniform distribution, to be 13 MHz (quoted from Reference [15] page 45 and 46), together orders of magnitude larger then the expected signal process rate.

Since the beam-related and cosmic background has several components (including synchrotron radiation, Coulomb scattering, inelastic Bremsstrahlung, the Touschek-effect, and cosmic rays) which are difficult to simulate precisely, non-collision data samples are used to estimate these contributions. A loose pre-selection for pure neutral final states - similar to the selection procedure for the signal process $e^+e^- \to n\bar{n}$ - is applied. Events without charged tracks in the MDC and at least one shower in the EMC within $|\cos\theta| < 0.75$ and an energy deposition above 0.5 GeV are selected. Events passing these selection criteria are investigated for their MUC response, i.e. for their last MUC layer with a response of the total 9 layers of resistive plates. With this approach it is possible to distinguish between particles coming from the Interaction Point (IP) and such coming from the outside of the detector.

Supplementary Figure 6 shows an example for the last layer with a response in the MUC using the loose pure neutral final state selection as described above. By applying a criterion on the last layer with a response (layers are associated with running ID's from the inner to the outer one), cosmic rays and a considerable amount of the other beam-related background events can be effectively suppressed.

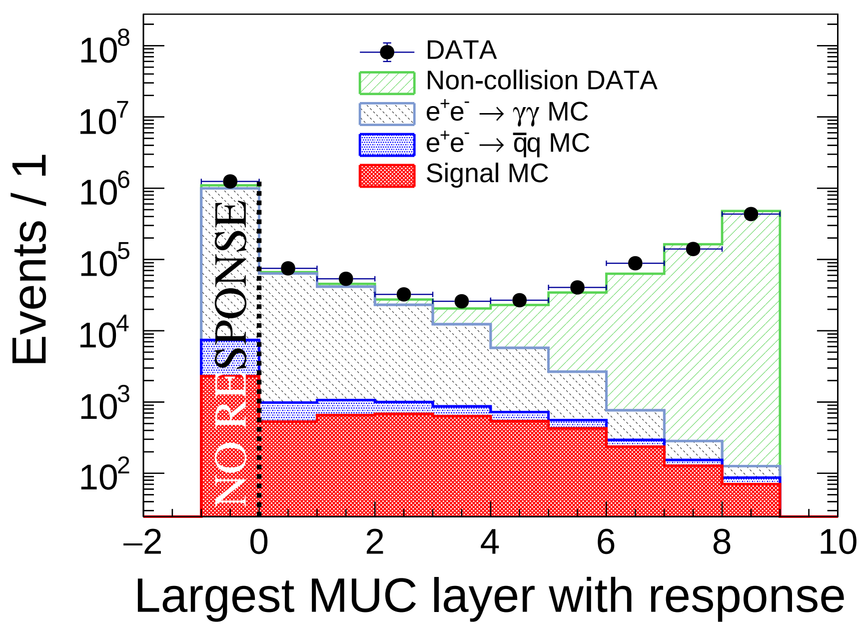

Supplementary Figure 6: The last layer with a response among the resistive plates of the MUC for events passing the pre-selection at $\sqrt{s} = 2.396$ GeV. Black dots with error bars represent the distribution from collider data, the histogram in red is the signal MC simulation for $e^+e^- \to n\bar{n}$, the light blue histogram is MC simulation for $e^+e^- \to \gamma\gamma$ background, the dark blue histogram shows the MC simulation for $e^+e^- \to q\bar{q}$, the green histogram is the distribution from beam-related background using combined samples at 2.2324 and 2.6444 GeV. Events with a layer ID's below zero separated by the dashed black line have no response in the MUC. The uncertainties are statistical and correspond to a 68.3% confidence level of a normal distribution.

Verification of the Analysis Methods with the Process $J/\psi \to n\bar{n}$

The signal event classification strategies A, B, and C for the process $e^+e^- \to n\bar{n}$ are tested with the process $e^+e^- \to J/\psi \to n\bar{n}$, as it follows the same kinematics. We use two data sets which have been collected with the BESIII detector at the c.m. energy of the J/ψ meson. The total number of the J/ψ events in the data samples is $(223.7 \pm 1.4) \times 10^6$ and $(1086.9 \pm 6.0) \times 10^6$ as quoted from the Supplementary Reference 1[a]. The number of signal events for $J/\psi \to n\bar{n}$ is determined similar to the main analysis after the category individual selection by fitting ΔT_n or $\sphericalangle_{\bar{n}}^{n}$ as shown in the Supplementary Figure 7.

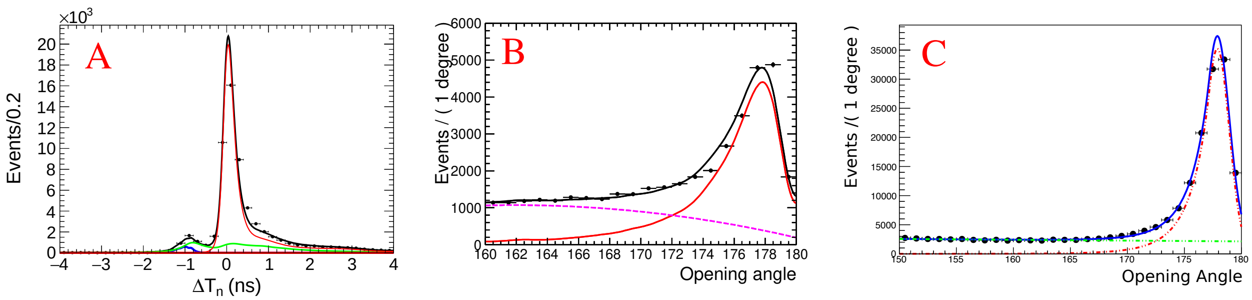

Supplementary Figure 7: (Left) Category A: determination of the signal events via a fit to the observable ΔT_n for the selected data at $\sqrt{s} = 3.097$ GeV. Black points represent collider data, the red line represents the signal shape obtained from $J/\psi \to \bar{n}n$ signal MC generated with CONEXC, the green line represents the sideband background, and the blue line represents the $e^+e^- \to \gamma\gamma$ background. The black line represents the combined fit model. (Middle) Category B: determination of the signal events via a fit to the observable $\sphericalangle_{n}^{\bar{n}}$ for the selected data at $\sqrt{s} = 3.097$ GeV. Black points represent collider data. The red line represents the signal shape obtained from signal MC ($e^+e^- \to J/\psi \to \bar{n}n$), the magenta line represents the background shape, the black line represents the combined fit model. (Right) Category C: determination of the signal events via a fit to the observable $\sphericalangle_{n}^{\bar{n}}$ for the selected data at $\sqrt{s} = 3.097$ GeV. Black points represent collider data, the red line represents the signal shape obtained from signal MC ($e^+e^- \to J/\psi \to \bar{n}n$) generated with CONEXC, the green line represent the beam-related and cosmic background. The blue line represents the combined fit model. For all data points the shown uncertainty is statistical and corresponds to a 68.3% confidence level of a normal distribution.

The signal MC efficiency is corrected with the control samples $e^+e^- \to J/\psi \to p\bar{n}\pi^-$ and $e^+e^- \to J/\psi \to \bar{p}n\pi^+$, similar to the efficiency correction in the main analysis. We list the branching ratios (BR) from the obtained data as calculated for each category and compare our results to the published value from the Reference [41]. Our results are consistent with each other and with the world data reference, as shown in the Supplementary Table 5.

Supplementary Table 5: Determination of the branching ratio $BR(J/\psi \to n\bar{n})$ with the 3 different analyses (as defined in the main paper). The quoted uncertainties for results from category A, B, and C are statistical.

Category	A	B	C	Reference [41]
$BR(J/\psi \to n\bar{n})(\times 10^{-3})$	2.02 ± 0.01	2.07 ± 0.03	2.00 ± 0.06	2.07 ± 0.01

[a] Supplementary Reference 1: M. Ablikim *et al.* (BESIII Collaboration), "Determination of the number of J/ψ events with inclusive J/ψ decays", Chin. Phys. C **41**, 013001 (2017).

Study of the Oscillation in the Effective Form Factor of the Neutron

Initially, the oscillation of the effective form factor $|G|$ is studied for the individual neutron data. Following the approach from Reference [24], a fit with a modified dipole function $G_{D^*}(q^2) \equiv G_{D^*}$ is performed,

$$G_{osc}(q^2) = |G_n| - G_{D^*}, \qquad G_{D^*} = G_D \cdot \frac{1}{1+\frac{q^2}{m_a^2}}, \qquad G_D = \frac{\mathscr{A}_n}{\left(1-\frac{q^2}{0.71(\mathrm{GeV}^2)}\right)^2}, \tag{1}$$

and the parameters are determined to $\mathscr{A}_n = 3.5 \pm 0.1$ and $m_a^2 \sim 50 \times 10^6$. The very large parameter for m_a^2 indicates that the data can be described by the common dipole formula G_D with the normalization $\mathscr{A}_n = 3.5 \pm 0.1$. Supplementary Figure 8(a) shows the two different parameterizations as blue and red dashed lines overlaying each other for comparison.

With the obtained parameter for G_D, the reduced form factor G_{osc} is studied for deviations from zero. To describe the oscillation in G_{osc}, a fit with Equation 6 is performed. The parameterization can describe the data well with $\chi^2/ndf = 11.8/13$, as shown in the Supplementary Figure 8(b). The obtained parameter for the momentum frequency is with $C^n = 5.28 \pm 0.36$ GeV^{-1} similar to frequency of $C^p = 5.5 \pm 0.2$ GeV^{-1} which has been extracted with the proton data as discussed in Reference [24]. For comparison, the shared momentum frequency from the simultaneous fit to the neutron and proton data is $C = 5.55 \pm 0.28$ GeV^{-1}, as discussed in the main paper.

To investigate the significance of the oscillation, the hypothesis of oscillation is tested versus a Null hypothesis. The fit with Equation 6 for the description of oscillation is tested against a constant fit (indicating a perfect agreement of the data with the dipole parametrization), as shown in the Supplementary Figure 8(b). The obtained statistical significance of the periodic structure is determined to 6.3σ.

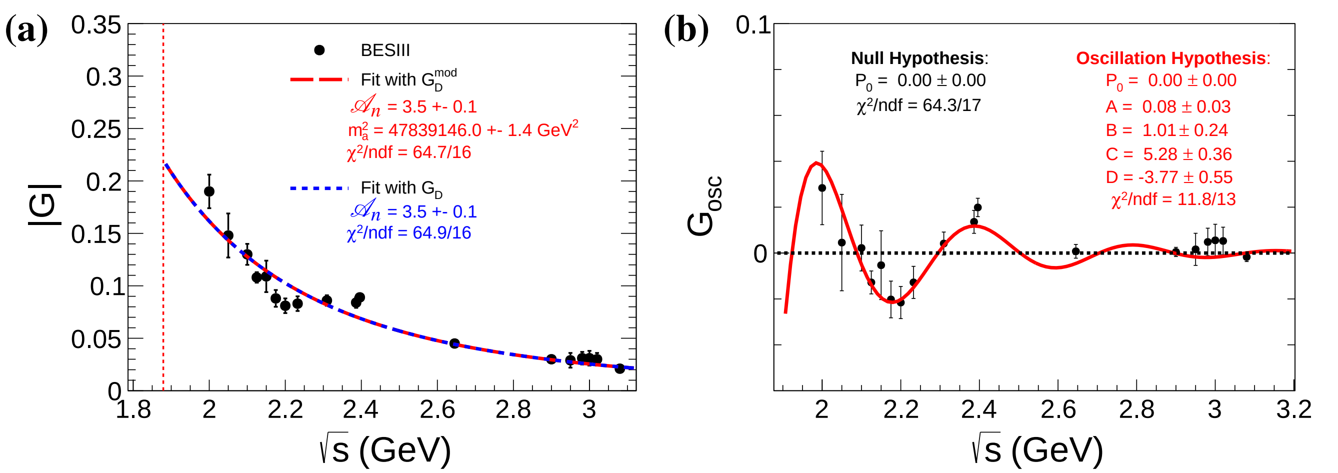

Supplementary Figure 8: Investigation of a possible oscillation from the effective form factor of the neutron. (Left) Fit with Supplementary Equation 1 to the effective form factor of the neutron $|G|$. The blue and red dashed lines are fits with the nominal and modified dipole formula, respectively. The parameters in the plot are obtained from the optimizations of the two fit functions. (Right) The fit with Equation 6 to G_{osc} is shown as the red solid line. Also shown is the fit with a constant fixed to zero as the Null hypothesis (black dotted line). The statistical significance for the oscillation is determined by comparison of the hypotheses, and is 6.3σ. The obtained parameters are shown in the plots. For all data points the total uncertainty (quadratic sum of statistical and systematic errors, corresponding to a 68.3% confidence level of a normal distribution) is plotted.